THE JOURNAL OF BIOLOGICAL CHEMISTRY VOL. 286, NO. 52, pp. 44799–44810, December 30, 2011

Novel p65 Binding Glucocorticoid-induced Leucine Zipper Peptide Suppresses Experimental Autoimmune Encephalomyelitis

Received for publication, July 4, 2011, and in revised form, September 19, 2011 Published, JBC Papers in Press, September 30, 2011, DOI 10.1074/jbc.M111.279257

Mythily Srinivasan[1] **and Srihari Janardhanam**

From the Department of Oral Pathology, Medicine and Radiology, School of Dentistry, Indiana University-Purdue University Indianapolis, Indianapolis, Indiana 46202

Background: Glucocorticoid-induced leucine zipper (GILZ), a glucocorticoid inducible molecule, physically binds and inhibits nuclear factor-κB (NF-κB).
Results: A peptide mimic derived from the p65 binding carboxyl terminus of GILZ inhibits T cells and prevents autoimmune encephalomyelitis.
Conclusion: GILZ-p65 interaction is a potential target for multiple sclerosis.
Significance: GILZ-peptide may provide a lead for small molecule NF-κB inhibitors.

Multiple sclerosis (MS) is a neurological disease characterized by inflammatory demyelination in the brain and spinal cord. The immune-mediated inflammation involves well orchestrated intermolecular interactions that exhibit rapid binding kinetics. The binding interfaces of transient interactions frequently include proline residues that favor an extended conformation for molecular recognition. Linear interface peptides are excellent lead inhibitors of specific protein-protein interactions because only small segments of the interface contribute to the binding. Glucocorticoid-induced leucine zipper (GILZ), a recently identified molecule exhibits potent anti-inflammatory properties. Mechanistically, a proline-rich segment in the carboxyl terminus of GILZ physically binds the p65 subunit of nuclear factor-κB and inhibits the transactivation of inflammatory cytokines. Integrating knowledge derived from the mechanism of action of GILZ with *in silico* structure prediction identified an immunomodulatory peptide, the GILZ-P. Treatment with GILZ-P exhibited therapeutic efficacy in experimental autoimmune encephalomyelitis, a model for human MS.

Multiple sclerosis (MS)[2] is a chronic immune-mediated inflammatory disease of the central nervous system characterized by relapsing-remitting clinical manifestations (1). At the molecular level, immune responses involve well orchestrated low affinity but high specificity intermolecular interactions that regulate intercellular communications and intracellular signaling pathways (1, 2). A common structural theme in the interfaces of transient protein interactions is the frequent presence of proline residues. Although the function of proline is to bring the proteins together so as to make subsequent interactions probable, the adjacent residues determine the specificity (3, 4). Greater than 60% of the mouse and human proteome exhibit at least one proline-rich motif (5). The high preponderance of proline-rich regions in the interfaces of proteins involved in critical biological processes suggests that these motifs could represent an important group of targets for therapeutic interventions (4).

The imino group of the proline side chain limits the rotation around the Cα bond by the covalent link and its Cδ atom sterically restricts the preceding residue to the β region of the Ramachandran map promoting a distinct secondary structure called polyproline type II (PP_{II}) helix (3, 6). The advantages of the PP_{II} helical structure for molecular recognition are the flexibility and orientation freedom offered by the extended conformation (3, 6). A conceptually straightforward strategy to develop specific inhibitors of protein-protein interactions is the synthesis of interface peptides derived from the primary sequence of one of the protein binding partners (4). Examples of linear peptides exhibiting PP_{II} conformation include peptides derived from the p85 subunit of PI 3-kinase, CD28-CDR-3 peptide, and protein kinase inhibitors (7–9).

Glucocorticoid-induced leucine zipper (GILZ) is a recently identified molecule during a systematic study of genes transcriptionally induced by glucocorticoids (10, 11). Functionally the GILZ negatively regulates Ras signaling, suppresses proinflammatory cytokines, and modulates T cell activation (12, 13). Indeed, the anti-inflammatory activities of glucocorticoids have been attributed to the induced up-regulation of GILZ (14) and are thought to be mediated by its ability to inhibit nuclear factor κB (NF-κB), the master regulator of inflammatory responses (12, 15).

NF-κB is a heterodimer of p50 and p65 that remains as an inactive complex with the inhibitory IκB proteins in the cytoplasm of resting T cells. Following activation, the subunits translocate to the nucleus and mediate transactivation of inflammatory genes (16). GILZ has been shown to physically bind the p65 subunit through a protein-protein interaction and inhibit NF-κB. Mutational analysis localized the site of interac-

[1] To whom correspondence should be addressed: 1121 W. Michigan St., Indianapolis, IN 46202. Fax: 317-278-3018; E-mail: mysriniv@iupui.edu.
[2] The abbreviations used are: MS, multiple sclerosis; GILZ, glucocorticoid-induced leucine zipper; TAD, transactivation domain; EAE, experimental autoimmune encephalomyelitis; MBP, myelin basic protein; DSIP, δ sleep-inducing peptide; LNC, lymph node cells.

tion with the p65 to the proline-rich carboxyl terminus of GILZ (GILZ-COOH) (14, 17). Structurally the p65 has an amino-terminal Rel homology domain, a nuclear localization sequence masked by the IκB inhibitory complex and a carboxyl-terminal transactivation domain (TAD) (18). It has been shown that the GILZ-induced inhibition of NF-κB does not require other rel proteins and is independent of IκB/NF-κB binding (12, 14, 17). This suggests that the GILZ:p65 binding does not involve the dimerizing rel homology domain or the nuclear localization sequence but is potentially mediated through the p65-TAD. Among the proteins that bind p65, a subset interacts directly with the TAD. Binding of the p65-TAD with other co-factors modulates the basal transcriptional machinery involved in cell cycle regulation and signaling (19). Interestingly, many p65-TAD interactants including p300, CBP (cAMP-response element-binding protein) (20), silencing mediator of retinoic acid and thyroid hormone receptors (SMRT) (21), A07 (22), and the TATA box-binding protein-associated factor 80 ($TAF_{II}80$) (23) exhibit proline-rich regions in the binding interface (Table 1).

In this study, we integrated molecular interactions of GILZ with *in silico* structure prediction to identify an immunomodulatory GILZ-peptide, the GILZ-P. Our data show that the GILZ-P potentially adopts the PP_{II} helical conformation and binds p65 and inhibits its nuclear translocation thereby suppressing T cell responses in experimental autoimmune encephalomyelitis (EAE), a model for human MS (24).

EXPERIMENTAL PROCEDURES

Molecular Modeling—Homology models of GILZ were developed using web-based systems CPHModels (25), Geno3D (26), SWISS-MODE (27), and I-Tasser (28). The primary structure of GILZ is highly homologous with that of the human δ sleep-inducing peptide (DSIP) (10, 11), the solution structure of which (PDB code 1DIP) was used as the template for the GILZ models (29). The predicted models were assessed for quality by QMEAN (Qualitative Model Energy Analysis), a comprehensive scoring system that determines the statistical probability for the agreement of predicted and calculated secondary structure and solvent accessibility (30). The secondary structure assignment of the GILZ models was independently assessed by the PROSS (Protein dihedral angle-based Secondary Structure assignment) program (31). Superimposition of the predicted GILZ models with the experimentally determined PP_{II} helix was performed to evaluate the similarity between the structures in terms of root mean square deviation.

Peptides and Reagents—GILZ-$P^{115-137}$ and a control peptide (control-P) of scrambled residues were synthesized as peptide amides and the $PLP_{139-151}$ (HSLGKWLGHPDKF) and MBP_{89-97} (VHFFKNIVTPRTP) as peptide acids (32). The amino-terminal of GILZ-P, control-P, and MBP_{89-97} were acetylated. All peptides were 95% pure as confirmed by mass spectrometry. Recombinant human p65 protein (r-p65) and purified r-GILZ with C-terminal DDK (catalog number TP320780) and biotinylated anti-DDK antibody were from OriGene Technologies Inc., Rockville, MD. Partial length p65 (p65ΔC14) and anti-p65 mAb were from Active Motif, Carlsbad, CA. Recombinant mouse GILZ protein and the mouse

TABLE 1

The table represents a compilation of cofactors of RelA/p65 shown to interact via the p65 TAD, together with evidence for these interactions

Data were collected via literature searches. Proline-rich motifs in the interacting regions of the co-factors were identified by hits via the ExPasy Bioinformatics Resource Portal. The *E*-value is the number of matches with a score equal to or greater than the observed score that are expected to occur by chance. RelA/p65 TAD:co-activator interacting proteins exhibit a proline-rich region in the interface.

Protein	Experiment	Interacting region	PRR in the interacting sequence	*E*-value	Ref.
A07	*In vitro* cell-based pull-down assay	C-terminal amino acid sequence 341–459	Pro^{262}-Pro^{447}	$1.2\ E^{-2}$	19
p300	Mammalian two-hybrid system	C-terminal amino acid sequence 1582–2414	Pro^{1842}-Pro^{2013}	$2.7\ E^{-11}$	17
CREB-binding protein (CBP)	Mammalian two-hybrid system	C-terminal amino acid sequence 1892–2441	Pro^{1878}-Pro^{2064}	$8.2\ E^{-12}$	17
			Pro^{2346}-Pro^{2385}	$5.9\ E^{-2}$	
TATA box-binding protein-associated factor 80	Co-immunoprecipitation	C-terminal sequence	Pro^{487}-Pro^{677}	$6.8\ E^{-05}$	20
Silencing mediator of retinoic acid and thyroid hormone receptors	Mammalian two-hybrid system	C-terminal amino acid sequence 1060–1495	Pro^{749}-Pro^{1097}	$5.3E^{-17}$	18
Glucocorticoid-induced leucine zipper	*In vitro* cell-based pull-down assay	C-terminal amino acid sequence 113–137	Pro^{115}-Pro^{132}		11, 15

anti-GILZ mAb (catalog number H00001831-M02) were from Abnova Corporation, Walnut, CA. The mouse anti-GILZ mAb exhibits cross-reactivity with the human GILZ. The chariot peptide Pep-1 (33, 34) was obtained from Anaspec, San Jose, CA.

GILZ:p65 Binding—High binding ELISA plates coated with 40 μM r-p65/r-GILZ were probed with cytoplasmic/nuclear extracts, respectively, of CD4+ peripheral blood mononuclear cells stimulated with purified protein derivative (10 units/ml) for 48 h in the presence of dexamethasone (100 μg/ml). Binding of the plate-bound r-p65 with cytoplasmic GILZ and the plate-bound GILZ with nuclear p65 was detected with anti-GILZ mAb or anti-p65 mAb, respectively, followed by trinitrobenzene substrate. For detecting direct interaction of r-GILZ (5–40 μM), captured wells were probed with r-p65 (0.325–40 μM) at 22 °C for 2 h and detected with peroxidase-conjugated anti-GILZ mAb followed by trinitrobenzene substrate. Alternatively plates coated with GILZ-P, control-P (3.9–250 μM), r-GILZ (0.2–1.8 μM) were probed with 40 μM r-p65:DDK/p65ΔC14 and detected with anti-DDK/anti-p65 mAb, respectively. Absorbance at 650 nm was measured between 0 and 300 s with a mixing time of 0.30 s and a 5-s interval between readings.

Data Analysis—The kinetic velocity or the slope of absorbance *versus* time curve was calculated by linear regression. The dissociation constant of the interaction between the r-p65 and r-GILZ/GILZ-P was determined as described (35, 36). A fraction of the bound r-p65 (x) and the ratio of bound r-p65 to the free r-GILZ/GILZ-P (y) were determined by the equations: $x = (A_o - A)/(A_{o)),\ where}\ A_o$ is the absorbance of r-p65·anti-p65 complex in the absence of bound r-GILZ/GILZ-P and $y = (A_o - A/A_o)/(a_o - i_o \times A_o - A/A_o)$, where a_o is the total concentration of r-GILZ/GILZP and i_o is the total concentration of r-p65 (36). K_D for the interaction was determined by the Scatchard equation: $x = 1 + K_D/y$.

Treatment of R-EAE—Groups of 8–10-week-old SJL/J female mice induced with EAE were administered intraperitoneally with vehicle/Pep1 (0.3 μM/mouse) mixed with r-GILZ (2 ng/mouse), of GILZ-P, or control-P (500 μg/mouse) in 100 μl of PBS on the day of immunization (day 0). A group of mice received the GILZ-P·Pep-1 complex 12 days post-immunization. Because the mouse and human GILZ proteins are highly identical (10, 11), rh-GILZ was used to evaluate the effect in R-EAE.

Pep-1-mediated Delivery—For Pep-1-mediated delivery, complexes of Pep-1·r-GILZ at varying proportions (50:1 μM to 1.25:1 μM or 10:5 μM in PBS) were incubated at room temperature for 30 min. Jurkat T cells were cultured in complete HL-1 medium supplemented with 5% fetal bovine serum, 25 mM HEPES, 2 mM L-glutamine, 50 units/ml of penicillin, 50 mg/ml of streptomycin, and 5×10^{-5} M β2-mercaptoethanol in a humidified chamber containing 5% CO_2 at 37 °C for 24 h. The cells were then rested for 2 h, washed, and cultured in a 96-well culture plate at 1×10^4 cells/well in serum-free medium for 60 min. Confluent T cells were then overlaid with the preformed Pep-1·GILZ complexes and incubated at 37 °C for 1 h. The cells were then extensively washed, permeabilized, and incubated with phycoerythrin-labeled anti-DDK for 30 min at 4 °C. Subsequent to washing, the cells were fixed in PBS, 2% paraformaldehyde. The efficiency of r-GILZ intracellular delivery was assessed by measuring the mean fluorescence intensity using FACS Calibur flow cytometer (BD Biosciences).

Proliferation and Cytokine Assays—The LNC/splenocytes were harvested 10 and 45 days post-immunization from R-EAE mice administered vehicle, r-GILZ, control-P, or GILZ-P on days 0 and 12 or left untreated. CD4+ cells isolated by microbead separation were cultured in a transwell system with irradiated syngenic splenocytes as APC in complete HL-1 medium and restimulated with 40 μg/ml of $PLP_{139-151}$, MBP_{87-99} or both, and ova in the presence or absence of dexamethasone (10^{-7}-20^{-7} M), r-GILZ (100–200 ng), GILZ-P (125–500 μM), or control-P (500 μM) preincubated with Pep-1 at a 1:20 M ratio for 20 min with Pep-1 alone. Supernatants collected at 24 and 48 h were assessed for specific cytokines using the OptEIA kits (BD Biosciences). Proliferation assays included parallel cultures for 72 h with a final 18-h pulse with [^{3}H]thymidine measured by liquid scintillation counting (Microbeta, Turku, Finland).

NF-κB Assay—5 μg of nuclear extracts isolated from $PLP_{139-151}$ restimulated CD4+ cells from R-EAE mice were incubated in a 96-well plate coated with oligonucleotides containing the NF-κB consensus binding site. The activated NF-κB bound to DNA was detected by anti-p65 antibody followed by a peroxidase-coupled secondary antibody and substrate using the TransAM kit protocol (Active Motif).

Real-time Polymerase Chain Reaction (RT-PCR)—50 ng of cDNA from CD4+ cells from R-EAE mice restimulated with $PLP_{139-151}$ for 24 h was amplified by RT-PCR using the SYBR Green/ROX qPCR master mixture (SABiosciences, Frederick, MD) on the ABI Prism 7000 (Applied Systems, Foster City, CA) as per the manufacturer's recommendations. The primers included: β2-microglobulin, forward, 5′-TCACTGACCGGCCTGTATGCTATC-3′, reverse, 5′-GTGAGGCGGGTGGAACTGTGT-3′; T-bet, forward, 5′-TCCCATTCCTGTCCTTCA-3′, reverse, 5′-GCTGCCTTCTGCCTTTC-3′; GATA-3, forward, 5′-ACCACGGGAGCCAGGTATG-3′, reverse, 5′-CGGAGGGTAAACGGACAGAG-3′; IL-10, forward, 5′-CCAGTTTTACCTGGTAGAAGTGATG-3′, reverse, 5′-TGTCTAGGTCCTGGAGTCCAGCAGACTC-3′; and FOX-P3, forward, 5′-GTGGTCAGCTGGACAATCAC-3′, reverse, 5′-CTGAGGCACCTGTTTTAGCA-3′. The magnitude of change in the mRNA was expressed by the method of $2^{-\Delta\Delta Ct}$ with untreated controls as the reference samples (24).

Statistical Analysis—A one-way analysis of variance with Tukey's post hoc test were performed to determine the statistical differences between the groups.

RESULTS

The Rationale and Design of GILZ-peptide—The primary sequence of GILZ consisting of an amino-terminal leucine zipper (LZ) motif and a proline-rich carboxyl terminus is highly homologous with that of the evolutionarily conserved TGFβ-stimulated clone 22 gene (*TSC-22*) and the porcine DSIP (Fig. 1*A*) (10, 11). Homology modeling of the human and mouse GILZ was performed by the CPHmodel, Geno 3D, Swiss Model,

and I-Tasser programs using the solution structure of the DSIP (PDB code 1DIP) as the primary template. Comparative analysis by QMEAN (30) suggested that equivalent models were generated by all four programs (Fig. 1*B*). The LZ domain of GILZ was shown to adopt an α-helical conformation and the proline-rich carboxyl terminal was predicted to be flexible (Fig. 1, *C–E*).

A

```
Mouse GILZ    1DLVKNHLMYAVREEVEVLKEQIRELLEKNSQLERENTLLKTLASPEQLEKFQSRL----S
Human GILZ     DLVKNHLMYAVREEVEILKEQIRELVEKNSQLERENTLLKTLASPEQLEKFQSCL----S
Human TSC22    DLVKSHLMYAVREEVEVLKEQIKELIEKNSQLEQENNLLKTLASPEQLAQFQAQLQTGSP
Porcine DSIP   DLVKNHLMYAVREEVEILKEQIRELVEKNSQLERENTLLKTLASPEQLEKFQSRL----S
Human DIP      DLVKNHLMYAVREEVEILKEQIRELVEKNSQLERENTLLKTLASPEQLEKFQSCL----S

Mouse GILZ   115PEEPAPEAPETPETPEAPG----GSAV137
Human GILZ     PEEPAPE---SPQVPEAPG----GSAV
Human TSC 22   PATTQPQG--TTQPPAQPASQGSGPTA
Porcine DSIP   PEEPAPE---TPEAPEAPG----GSAV
Human DIP      PEEPAPE---SPQVPEAPG----GSAV
```

B

Structure	Q Mean6 Score	
	Raw Score	Z score
1 DIP (Template)	0.567	-2.13
CPH Models		
Human GILZ	0.485	-1.93
Mouse GILZ	0.501	-1.80
SWISS-Model		
Mouse GILZ	0.668	0.26
Human GILZ	0.469	-1.89
I-TASSER		
Model 1	0.325	-4.72
Model 2	0.382	-4.08
Model 3	0.341	-4.54
Model 4	0.476	-3.00
Model 5	0.556	-2.09
GENO-3D		
Model 1	0.435	-2.13
Model 2	0.435	-2.14
Model 3	0.420	-2.25
Model 4	0.363	-2.65
Model 5	0.452	-2.01
Model 6	0.378	-2.54

F

Structure	RMSD		Phi	psi	%PP_{II} helix
1 DIP	3.5A	Pro 61 Pro 72	-78.9 -78.3	142.3 149.8	7.8
		GILZ Residue (mouse)			
CPH MODEL					
Mouse GILZ	3.03 A	Pro120	-73.1	165.9	7.5
Human GILZ	3.15 A	Pro120 Pro129	-64.0 -73.3	149.8 146.5	7.5
SWISS MODEL					
Mouse GILZ	3.49 A	Pro 118 Pro 129	-78.9 -78.3	142.3 149.8	7.0
Human GILZ	3.69 A	Pro 118 Pro 123	-64.6 -68.4	174.1 144.8	2.6
Geno 3-D Models					
Model 1	2.96 A	Pro120 Pro 123	-63.9 -64.0	180 128.4	7.8
Model 2	3.01 A	Pr0 123	-64.0	124.8	3.9
Model 3	2.99 A	Pro123 Pro126	-64.1 -52.9	123.6 130.7	3.9
Model 4	3.27 A	Pro 123 Pro 126	-64.1 -52.9	123.6 130.7	7.8
Model 5	3.01 A	Pro 120 Pro 123	-63.2 -67.6	177.5 132.8	9.1
Model 6	2.92 A	Pro 120 Pro 123	-64.1 -69.3	173.8 128.4	0
I-Tasser Models					
Model 1	3.50 A	Pro ^{120} Pro ^{123} Ala ^{128}	-63.0 -71.8 -77.2	156.9 180 124	0.08
Model 2	3.54 A	Pro 115 Pro 120	-57.5 -69.6	127.6 138.9	0.07
Model 3	3.62 A	Val 125 Glu 127	-65.4 -68.8	121.4 139.1	0.05
Model 4	3.39 A	Pro 120 Gln 124	-73.9 -61.3	125.2 153.0	0.07

C

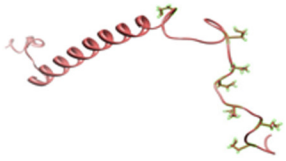

D

E

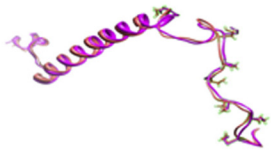

G

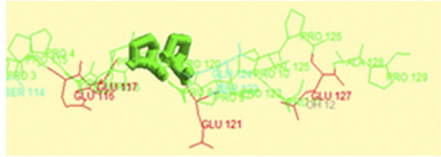

H

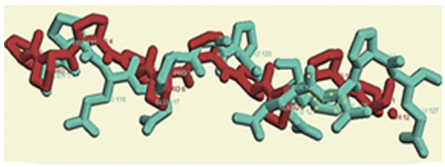

I

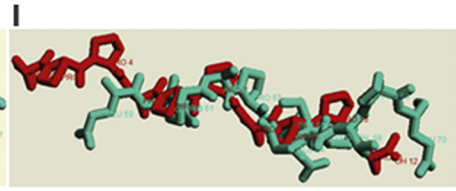

Often misrepresented as disordered regions due to the absence of intra-chain hydrogen bonds, proline-rich regions are known to favor the PP_{II} helical conformation (6). The extent of the PP_{II} helix is determined by the degree of backbone solvation and modulated by side chain interactions (6). The GILZ-COOH consists of a three $(PXX)_n$ motif with proline as every third residue (Fig. 1*A*). Secondary structure assignment based on backbone dihedral angles by PROSS showed that Pro^{120} of GILZ exhibited an ϕ angle of $-67 \pm 5°$ and ψ angle of $142.5 \pm 15°$ (Fig. 1*F*) adopting the PP_{II} helical conformation (6). Additionally, the presence of multiple glutamic acid residues in the region increases the net charge further promoting the extended conformation by electrostatic repulsion (37). Superimposition of the predicted GILZ over the experimentally determined PP_{II} helix yielded root mean square deviations of <5 Å, which suggests significant structural similarity (Fig. 1, *G–I*). Because the extended conformation is induced by local folding relatively independent of long range interactions, it is likely that the end groups that blocked the synthetic GILZ-P potentially adopts a PP_{II} helical conformation (6).

Kinetics of GILZ-peptide-p65 Interaction—We initially investigated the interaction between GILZ and p65 proteins by modified cellular ELISA. Treatment with dexamethasone increases GILZ expression and suppresses p65 translocation in activated T cells (14). Hence, the nuclear or cytoplasmic protein fractions derived from the CD4+ T cells stimulated with recall antigen in the presence of dexamethasone were assessed for binding plate-bound r-GILZ or r-p65, respectively. Although the absorbance was significantly increased in the r-p65-coated wells probed with the cytoplasmic fraction of dexamethasone-treated activated CD4+ T cells (Fig. 2*A*), it was significantly decreased in r-GILZ-coated wells probed with the nuclear fraction of CD4+ T cells activated in the presence of dexamethasone as compared with untreated cells (Fig. 2*B*). Reduced p65 in the nuclear fractions of cells treated with dexamethasone alone is consistent with its ability to inhibit NF-κB translocation in unstimulated cells (Fig. 2*B*).

To detect direct interaction, the ability of r-p65 to inhibit the binding of anti-GILZ mAb with the plate-bound r-GILZ was assessed. The GILZ·anti-GILZ complex formation was inhibited by r-p65 in a dose-dependent manner (Fig. 2*C*). To determine the kinetics of interaction between r-GILZ/GILZ-P and the p65, plate-bound r-GILZ, GILZ-P, and control-P at varying concentrations was probed with full-length r-p65-DDK. The percent of p65 binding decreased with decreasing concentrations of r-GILZ/GILZ-P (Fig. 2*E*). The adjusted velocity of the interaction between r-p65 and r-GILZ (7.5/s) or GILZ-P (25/s) was observed at 1:4 molar concentrations (Fig. 2, *F* and *G*). A plot of the change in absorbance with time showed that maximum absorbance was reached at a later time point in the binding of r-GILZ (210 s) than of GILZ-P (38 s) with r-p65 suggesting a slower association rate and hence weaker strength for the former interaction as compared with the latter (data not shown). Scatchard plot and linear regression analysis suggested that the dissociation constant, K_D, for the interaction between r-GILZ or GILZ-P and r-p65 were $5.91 \pm 2.4 \times 10^{-7}$ M (Fig. 2*H*) and $1.12 \pm 0.25 \times 10^{-6}$ M (Fig. 2*H*), respectively. Absorbance over background was not observed when plate-bound r-GILZ/GILZ-P was probed with p65ΔC14 and detected with anti-p65 mAb (Fig. 2*E*), suggesting that the GILZ-P potentially interacts selectively with the p65-TAD. Significant absorbance was not observed in wells coated with control-P and probed with r-p65/p65ΔC14 (Fig. 2*D*).

Pep-1-mediated Intracellular Delivery of r-GILZ in T Cells—For an effective intracellular concentration, r-GILZ/GILZ-P/control-P were mixed with an amphipathic chariot peptide, Pep-1, which rapidly associates through hydrophobic noncovalent interactions and forms stable nanoparticle complexes in solution independent of cargo sequence or size (Fig. 3, *A–C*) (34). The efficiency of Pep-1 to deliver biological molecules was investigated by incubating Jurkat T cells with preformed complexes of Pep-1 and r-GILZ at varying concentrations. Intracellular delivery was seen in cells incubated with a r-GILZ·Pep-1 complex but not in cells incubated with r-GILZ/Pep-1 alone (Fig. 3, *A–C*). The delivery was most efficient in cells incubated with Pep-1 and r-GILZ at the molar ratio of 50/20:1 as evidenced by the higher mean fluorescence intensity (Fig. 3*D*). The delivery efficiency decreased with decreasing concentrations of Pep-1 (Fig. 3*D*). The mean fluorescence intensity was equivalent in untreated cells and cells overlaid with r-GILZ/Pep-1 alone (Fig. 3*D*). Pep-1 has been effectively used for intracellular delivery of different cargos; including peptide inhibitors of protein kinases, apoptotic protein, and small interfering RNA (33, 34).

Effect of GILZ-peptide on T Cell Responses—To investigate the ability of GILZ-peptide to interfere with the GILZ-p65 interactions, *in vitro* T cell proliferation assays were performed. A significantly decreased proliferative response (mean Δcpm) was observed in CD4+ LNC isolated from R-EAE mice and re-stimulated *in vitro* with $PLP_{139-151}$ in the presence of dexamethasone/r-GILZ/GILZ-P with maximum inhibition in cultures treated with 250 μM GILZ-P (1404 ± 106). No significant

FIGURE 1. *A*, sequence alignment of human GILZ (BAB18680.1), mouse GILZ (AAD01789.1), human *TSC22* (CAA10951.1), porcine DSIP (AAB28177.1), and human DIP by CLUSTAL W (46). The conserved proline residues are highlighted. Homology modeling of mouse GILZ and human GILZ were generated based on sequence and structure similarity with the porcine δ sleep-inducing peptide (PDB 1DIP). *B*, validity of the models from CPH Models, Geno3D, Swiss Model, I-Tasser, and Geno3D were assessed with the QMEAN 6 program. The QMEAN 6 score is a composite score consisting of a linear combination of 6 terms (C-β interaction energy, all atom pairwise energy, salvation energy, torsion angle energy, secondary structure agreement, and solvent accessibility agreement). The pseudo-energies of the contributing terms (raw scores) are given together with their *Z*-scores with respect to scores obtained for high-resolution experimental structures of similar size solved by x-ray crystallography. *C* and *D* show the structure of PDB code 1DIP and a representative model of the mouse GILZ generated by Swiss Model. *E*, comparison by overlap yields a root mean square deviation of less than 0.1 Å between the mouse GILZ model and PDB code 1DIP suggesting excellent structural symmetry. *F* shows the values of the backbone dihedral angles depicting the secondary structure of the GILZ-COOH as assigned by PROSS. The torsion angles ϕ and π of Pro^{120} and Pro^{123} are consistent with the PP_{II} helical conformation in the predicted GILZ models. The root mean square deviation of the superimposition of the GILZ models against the x-ray crystal structure of the synthetic PP_{II} helix as determined by CHEMERA is also given. *G–I* show representative superimposed structures of synthetic PP_{II} in *gray* and the (*G*) CPH mouse-GILZ model, (*H*) Swiss Model mouse GILZ model, and (*I*) Geno-3D mouse GILZ model in *blue*. Pro^{120} and Pro^{123} are highlighted.

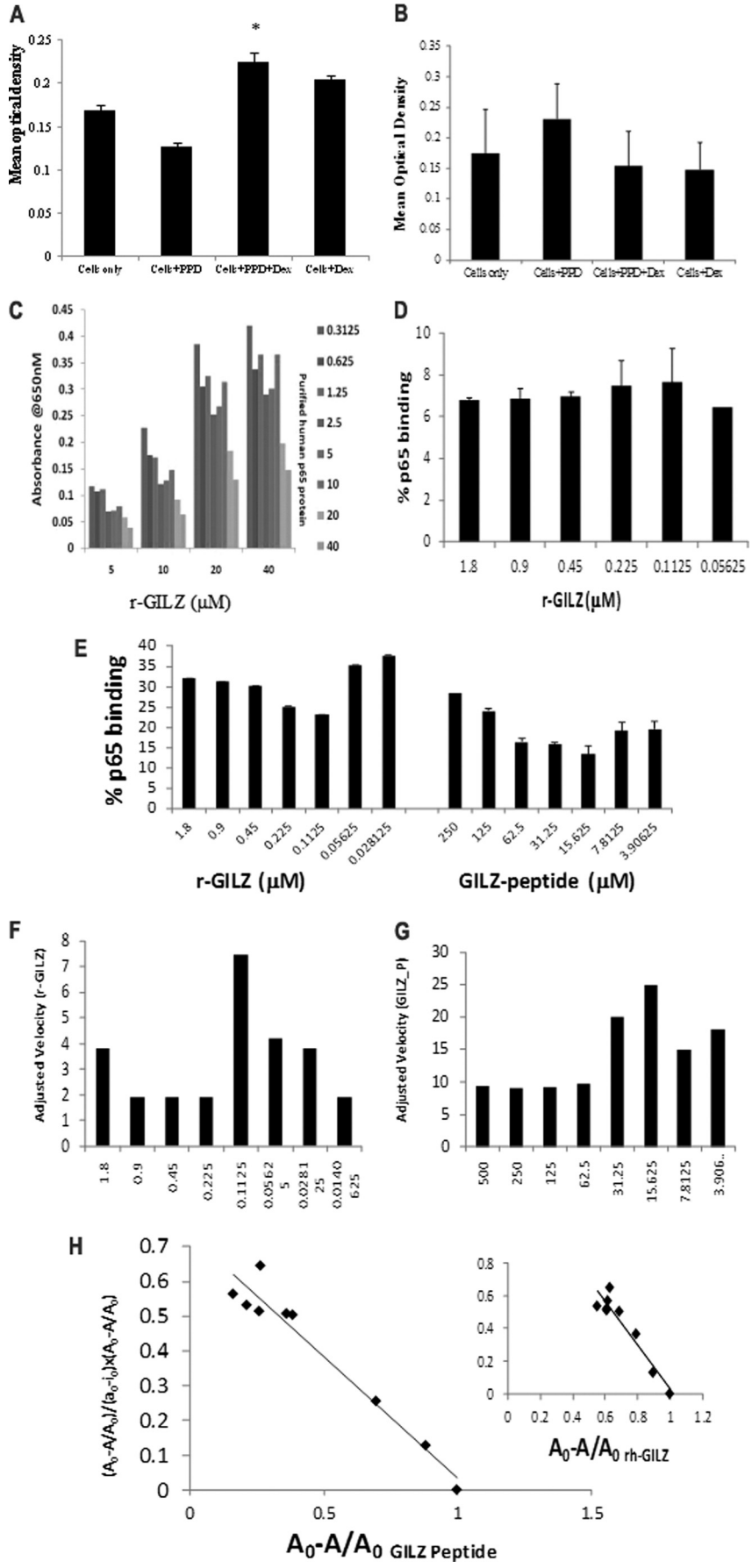
A
Mean optical density
Cells only
Cells+PPD
Cells+PPD+Dex
Cells+Dex
B
Mean Optical Density
C
Absorbance @650nM
Purified human p65 protein
r-GILZ (μM)
D
% p65 binding
r-GILZ(μM)
E
% p65 binding
r-GILZ (μM)
GILZ-peptide (μM)
F
Adjusted Velocity (r-GILZ)
G
Adjusted Velocity (GILZ_P)
H
A0-A/A0 GILZ Peptide
A0-A/A0 rh-GILZ

inhibition was observed in cultures treated with control-P (6079 ± 70), Pep-1 alone (6022 ± 87), or GILZ-P alone (6663 ± 173) (Fig. 3*E*). $PLP_{139-151}$ primed CD4+ cells did not exhibit a significant response to an irrelevant antigen, ova (418 ± 24).

We next investigated whether the GILZ-P-mediated reduction in proliferation is associated with the modulation of cytokine response and p65 transactivation. CD4+ LNC from $PLP_{139-151}$-primed mice re-stimulated *in vitro* in the presence of dexamethasone/GILZ-P/r-GILZ secreted significantly lower pro-inflammatory IFN-γ (Fig. 3*F*), IL-12 (Fig. 3*G*), and IL-17 (Fig. 3*H*) but elevated anti-inflammatory IL-10 cytokine (Fig. 3*I*) as compared with untreated/control-P-treated cells. Furthermore, *in vivo* primed CD4+ LNC re-stimulated with $PLP_{139-151}$ in the presence of dexamethasone/r-GILZ/GILZ-P exhibited significantly decreased T-bet mRNA (Fig. 3*K*), the canonical Th1 transcription factor, and elevated GATA-3 (Fig. 3*L*), the Th2 transcription factor, as compared with unstimulated/control-P-treated cells. Importantly, significantly decreased p65-specific DNA binding activity was observed in nuclear extracts of CD4+ LNC-restimulated with $PLP_{139-151}$ in the presence of dexamethasone/r-GILZ/GILZ-P as compared with untreated or control-P-treated cells (Fig. 3*J*).

GILZ-P Protects against R-EAE—The biological potential of GILZ-P during antigen priming *in vivo* was investigated in R-EAE. On day 0 groups of SJL/J mice were induced by R-EAE and administered a single intraperitoneal injection of PBS or a complex of Pep-1 and r-GILZ/GILZ-P/control-P. Separate groups of mice received a single dose of Pep-1·GILZ-P on day 12 post-immunization. The average clinical score per day was significantly lower in mice treated with GILZ-P (day 0/day12), r-GILZ as compared with the control groups (Fig. 4, *A* and *B*). The severity of clinical disease as suggested by the mean total clinical score was significantly lower in mice treated with GILZ-P (day 0, 2.25 ± 0.72; day 12, 15.75 ± 4.85) or r-GILZ (7.13 ± 2.8) as compared with vehicle (28.5 ± 5.57) or control-P (33 ± 7.5)-treated mice. Significantly, whereas the vehicle or control-P-treated mice exhibited clinical relapse after initial remission, the mice that received GILZ-P/r-GILZ exhibited minimal relapse and continued to be protected for the entire period of observation (Fig. 4*A*).

GILZ-peptide Suppresses T Cell Responses in R-EAE—To determine whether the protection mediated by GILZ-P is due to modulation of T cell responses, we assessed the functional responses of CD4+ splenocytes from R-EAE mice treated with PBS/r-GILZ/GILZ-P/control-P. Proliferative responses (mean Δcpm) to $PLP_{139-151}$ were significantly decreased in CD4+ splenocytes from mice treated with the r-GILZ (16,880 ± 264), GILZ-P (5,733 ± 208, day 0) as compared with that from vehicle (38,657 ± 533) or control-P (32,460 ± 940)-treated mice (Fig. 4*C*). The average proliferative response of unstimulated CD4+ splenocytes for vehicle, r-GILZ, GILZ-P (day 0), GILZ-P (day 12), and control-P-treated groups of mice was 2,695 ± 608, 2,037 ± 603, 2,376 ± 602, 1,823 ± 532, and 2,645 ± 425, respectively. No significant difference was observed in the proliferative responses of splenocytes to ovalbumin between the different treatment groups (Fig. 4*C*).

We next investigated the effect of *in vivo* GILZ treatment in inflammatory cytokine responses. Upon re-stimulation with $PLP_{139-151}$ the secretion of Th1 cytokines IL-12 and IFN-γ was significantly reduced in CD4+ splenocytes from mice treated on day 0 with r-GILZ (22.5 ± 01.05 and 100.5 ± 6.8 pg/ml, respectively) or GILZ-P (12.7 ± 0.47 and 96.5 ± 7.1 pg/ml, respectively) than from vehicle (53.3 ± 5.2 and 132.9 ± 7.6 pg/ml, respectively) or control-P (54 ± 4.2 and 111.8 ± 5.6 pg/ml, respectively)-treated mice (Fig. 4, *D* and *E*). Although IL-12 was significantly lower in CD4+ cells from mice treated with GILZ-P 12 days post-immunization, the reduction in IFN-γ was not significant as compared with that from control groups of mice. The IL-17 secretion by $PLP_{139-151}$ re-stimulated CD4+ cells from mice treated on day 0 with r-GILZ (10.66 ± 0.2 pg/ml) or GILZ-P (10.85 ± 0.3 pg/ml) was significantly decreased as compared with cells from vehicle (12 ± 0.7 pg/ml) or control-P (11.95 ± 0.11 pg/ml)-treated mice (Fig. 4*F*). In contrast, the anti-inflammatory IL-10 secretion was significantly increased in the $PLP_{139-151}$-stimulated cultures of CD4+ LNC from mice treated on day 0 with GILZ-P (2316 ± 52.9 pg/ml) as compared with that from vehicle (1456 ± 83.8 pg/ml) or control-P (1488 ± 22.9 pg/ml)-treated mice (Fig. 4*G*).

Because R-EAE is a relapsing disease secondary to epitope spreading (32), we evaluated the effect of GILZ-P on T cell cytokine responses to a second common encephalitogenic epitope in SJL/J EAE, the MBP_{89-97}. The MBP_{87-99}-stimulated CD4+ splenocytes from mice treated on day 0 with GILZ-P secreted significantly lower IL-12 (28.4 ± 1.6 pg/ml), IFN-γ (97.4 ± 6.9 pg/ml), and IL-17 (10.43 ± 0.4 pg/ml) as compared with vehicle/control-P treated mice (Fig. 4, *D–F*). Importantly, significantly elevated IL-10 cytokine was secreted by CD4+ splenocytes from mice treated on day 0 with r-GILZ (1667 ± 63.7 pg/ml) or GILZ-P (1850.8 ± 90 pg/ml) in response to MBP_{87-99} (Fig. 4*G*). Furthermore, MBP_{87-99} but not $PLP_{139-151}$ stimulation significantly increased TGF-β secretion by CD4+ splenocytes from mice treated on day 0 with GILZ-P (33.31 ± 4 pg/ml) or r-GILZ (31.7 ± 0.8 pg/ml) as compared with vehicle (25.3 ± 2.9 pg/ml) or control-P (11.8 ± 4.7 pg/ml)-treated mice (Fig. 4*H*). No significant difference was observed in the response of the CD4+ LNC from the different groups of mice to ova, a control antigen.

FIGURE 2. **GILZ-p65 binding analysis.** CD4+ cells from the peripheral blood mononuclear cells of individuals vaccinated with the BCG vaccine were stimulated with PPD in the presence or absence of dexamethasone. Nuclear and cytoplasmic extracts were obtained from cells harvested after 24 h. Binding between the plate-bound r-p65 and the cytoplasmic GILZ (*A*) or the plate-bound r-GILZ and nuclear p65 (*B*) were detected by anti-GILZ (*A*) or anti-p65 (*B*) mAb, respectively. *, $p < 0.05$ when compared with cells stimulated with antigen alone. *C*, wells coated with r-GILZ at increasing concentrations (5–40 μM) were probed with full-length r-p65:DDK at increasing concentrations (0.3125–40 μM) and detected with anti-human GILZ mAb (*D*). High Bind ELISA plates coated with increasing concentrations of GILZ-P (3.9–250 mM) or r-GILZ (0.2–1.8 μM) were probed with 40 μM r-p65 (*E*) or r-p65ΔC14 (*D*) and detected with anti-DDK (*E*) and anti-p65 mAb (*D*) followed by trinitrobenzene substrate. Absorbance was read at 605 nm over a period of time between 0 and 300 s with a mixing time of 0.30 s and a 5-s interval between readings prior to stopping. The velocity of r-GILZ-p65 (*F*) and GILZ-P-p65 (*G*) reactions was measured as mean optical density/min. Scatchard plot analysis of bound p65 ($A_o - A/A_o$) against the ratio of bound p65 to free r-GILZ/GILZ-P ($y = (A_o - A/A_o)/(a_o - i_o \times A_o - A/A_o)$) was used to determine the dissociation constant for the interaction between r-GILZ-p65 and GILZ-P and p65 (*H*).

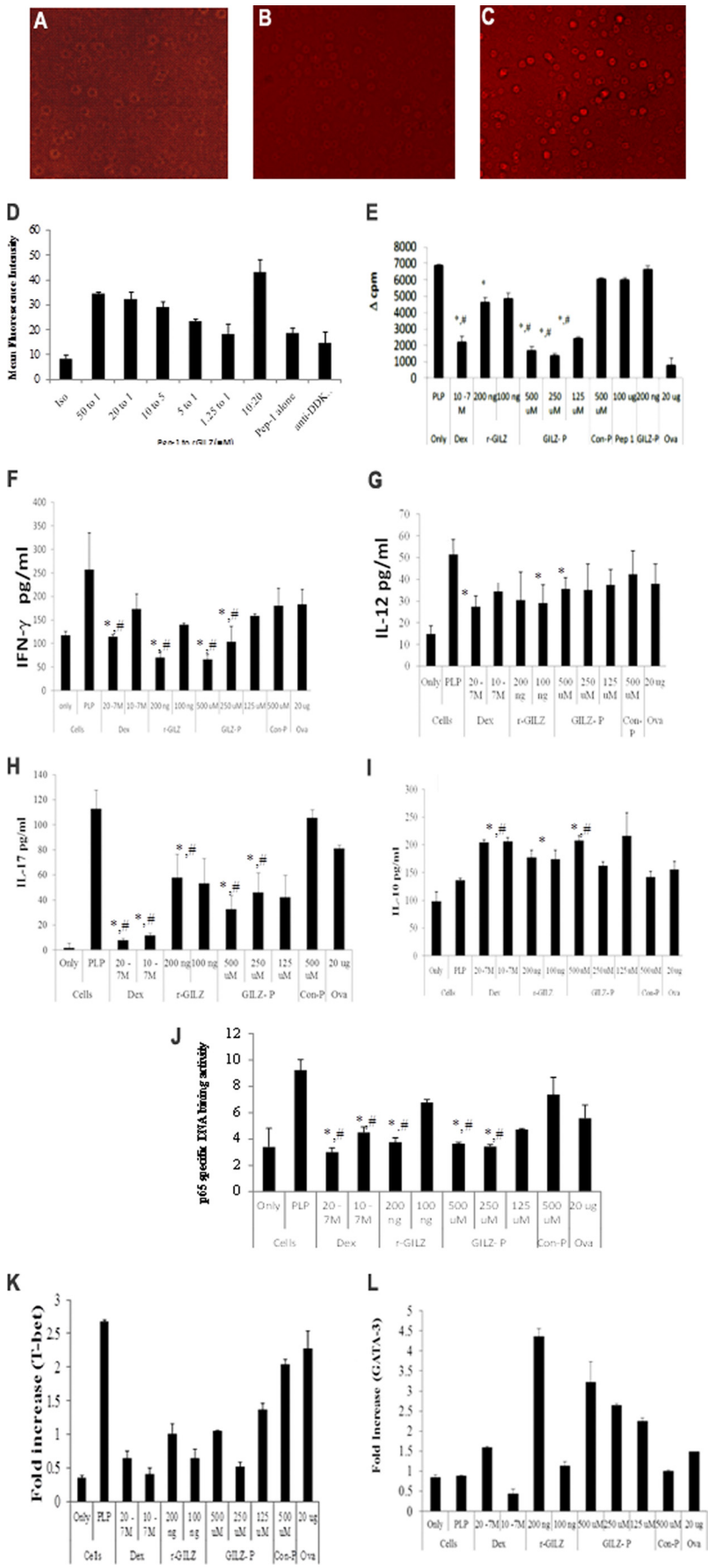
A
B
C
D
Mean Fluorescence Intensity
Iso
50 to 1
20 to 1
10 to 5
5 to 1
1.25 to 1
10:20
Pep-1 alone
anti-DDK...
E
Δ cpm
PLP
10 -7 M
200 ng
100 ng
500 uM
250 uM
125 uM
500 uM
100 ug
200 ng
20 ug
Only
Dex
r-GILZ
GILZ- P
Con-P
Pep 1
GILZ-P
Ova
F
IFN-γ pg/ml
G
IL-12 pg/ml
H
IL-17 pg/ml
I
IL-10 pg/ml
J
p65 specific DNA binding activity
K
Fold increase (T-bet)
L
Fold Increase (GATA-3)
Cells
Dex
r-GILZ
GILZ- P
Con-P
Ova

GILZ-peptide Increases Expression of Regulatory Molecules in T Cells in R-EAE—We next determined whether GILZ-peptide facilitates Th1 to Th2 skewing *in vivo* by modulating specific transcription factors, T-bet and GATA-3, respectively (24). RT-PCR showed that the CD4+ LNC from mice induced EAE and treated on day 0 with vehicle/r-GILZ/GILZ-P/control-P exhibited significantly lower T-bet but elevated GATA-3 mRNA following re-stimulation with $PLP_{139-151}$ (Fig. 5, *A* and *B*). GILZ has been shown to induce IL-10 secretion and promote regulatory T cell differentiation (15). Accumulation of FOXP3 + IL-10 secreting regulatory T cells in the CNS has been associated with disease recovery in EAE (38). We observed that the CD4+ T cells from mice treated on day 0 with r-GILZ/GILZ-P exhibited significantly higher expressions of IL-10 and FoxP3 mRNA as compared with that from vehicle/control-P-treated mice (Fig. 5, *C* and *D*).

DISCUSSION

In the panel of emerging therapeutic agents for human diseases synthetic peptides constitute highly attractive tools. The advantages of peptides include nonimmunogenicity, inexpensive production, and the potential for high specificity. Hence despite the drawback of poor stability, peptide therapeutics is rapidly advancing with over 190 peptides in phase I/II clinical trials for various diseases (39). In this study we report the identification of a novel p65 binding GILZ-peptide that exhibits therapeutic potential in R-EAE.

GILZ is a glucocorticoid responsive molecule that inhibits NF-κB transactivation (11, 17) by physically interacting with the p65 subunit via a short proline-rich segment. Secondary structure assignment showed that Pro^{120} of GILZ-P adopts an extended PP_{II} helical conformation providing a mechanism for discriminatory recognition without requiring high affinities (6). Consistent with this structural prediction previously, mutation of Pro^{120} has been shown to abrogate the GILZ-p65 interaction (14). Peptides derived from the proline-rich regions of proteins potentially exhibit similar affinity as the entire protein with the interacting partner (7, 8, 40). We show that the end groups that blocked GILZ-P bind the r-p65 with similar kinetics as the r-GILZ with the strength of interaction in the micromolar range commonly observed for transient intermolecular interactions.

Analyses of structural complexes of interactions wherein the binding depends on the presence of one or more prolines have shown that the functionally critical prolines in the interface of one protein often are in contact with aromatic residues from the other component (41). In this context, it is interesting to observe that the p65-TAD that potentially interacts with GILZ-COOH presents two highly conserved aromatic residues: Phe^{534} and Phe^{542}, which together with conserved acidic residues at Asp^{531} and Asp^{533} and phosphorylation sites at Ser^{529} and Ser^{536} constitute critical residues for p65 transactivation (18).

Although T cell activation has been shown to down-regulate GILZ, blockade of T cell receptor signaling or costimulation up-regulates GILZ expression in CD4+ T cells (24, 42). Transfection of *gilz* inhibits NF-κB activation, down-regulates T-bet, and suppresses IFN-γ secretion by activated CD4+ T cells (12, 13). In contrast, GILZ expression up-regulates Th2-specific transcriptional factors STAT-6 and GATA-3 and increases IL-4 secretion (13). Thus GILZ is thought to regulate an immune response by modulating the Th1/Th2 balance (14). Our data suggest that GILZ-P treatment mimicked many actions of GILZ. Restimulation of antigen-primed CD4+ T cells in the presence of GILZ-P suppressed p65 activation, T-bet transcription, and Th1 cytokines and enhanced GATA-3 and Th2 cytokines.

The diverse roles of GILZ in a range of cellular events implicated in the Th1-mediated pathology suggest that GILZ could represent an immunomodulatory target in the treatment of MS, rheumatoid arthritis, and inflammatory bowel disease (14). GILZ is observed abundantly in the rheumatoid synovium suggesting a role in the local regulation of chronic inflammation (43). Transgenic mice overexpressing *gilz* in T cells are protected against the Th1-mediated transfer of colitis (44). We observed that a single dose of r-GILZ or GILZ-P administered on the day of disease induction protected mice against R-EAE. Significantly when administered during active immune response against the inducing antigen (day 12) GILZ-P suppressed clinical symptoms suggesting an ameliorating effect on disease development. Importantly, treatment with GILZ-P suppressed clinical relapse in R-EAE. The reduced proliferative and cytokine response of the activated T cells to an encephalitogenic peptide of a myelin protein not used for disease induction suggests that the continued protection in R-EAE was presumably mediated by preventing epitope spreading.

FIGURE 3. *A–D*, intracellular delivery of r-GILZ by Pep-1:Jurkat T cells in serum-free HL-1 medium were overlaid with a pre-formed complex of r-GILZ (DDK tag) and Pep-1 at varying concentrations and incubated in a humidified chamber for 1 h at 37 °C. Intracellular delivery of r-GILZ was detected using phosphatidylethanolamine-labeled anti-DDK mAb in permeabilized cells and measured by FACS Calibur. Representative images of cells incubated with (*A*) r-GILZ alone, (*C*) 20:1 ratio of Pep-1 to r-GILZ, and (*B*) pep-1 alone are shown. The delivery efficiency was assessed by mean fluorescence intensity (*D*). Data are average of two different experiments ± S.E. *E–L*, treatment with GILZ-peptide suppress T cell responses. CD4+ splenocytes (5×10^5 cells/well) isolated from antigen-primed SJL mice were co-cultured with irradiated syngenic splenocytes as APC and restimulated with $PLP_{139-151}$ (40 μg/ml) for a total of 72 h (including an 18-h pulse with [^{3}H]thymidine) in the presence of dexamethasone ($20^{-7}/10^{-7}$ M), r-GILZ (100 and 200 ng), GILZ-P (125–500 μM), and control peptide (*C-P*)(500 μM) as shown. *E*, data represent mean Δcpm (cpm of the antigen-stimulated cells − cpm of cells only) ± S.D. from three different experiments. *F–I*, supernatants collected at 48 h were assessed for IFN-γ (*F*), IL-12 (*G*), IL-17 (*H*), and IL-10 (*I*) by ELISA. Data are presented as mean ± S.D. *J*, in separate experiments, draining LNC cultured similarly were harvested at the end of 24 h. Five micrograms of nuclear extracts were tested for binding of the activated p65 NF-κB subunit to an NF-κB consensus sequence using the TransAM NF-κB ELISA kit. The p65 DNA binding activity was calculated as the ratio of absorbance from $PLP_{139-151}$-stimulated cells to that of unstimulated cells. Values are the average ± S.D. performed 3 times in duplicate. *K–L*, real time PCR for T-bet (*K*) and GATA-3 (*L*) was performed using 50 ng of cDNA isolated from CD4+ LNC of R-EAE mice re-stimulated *in vitro* with $PLP_{139-151}$ under the indicated conditions. Treatment with dexamethasone, r-GILZ, and GILZ-peptide down-regulated T-bet (*K*) and up-regulated GATA-3 (*L*) expression in activated CD4+ T cells. * and #, $p < 0.05$ as compared with the cells treated with $PLP_{139-151}$ alone or cells stimulated in the presence of control-P, respectively.

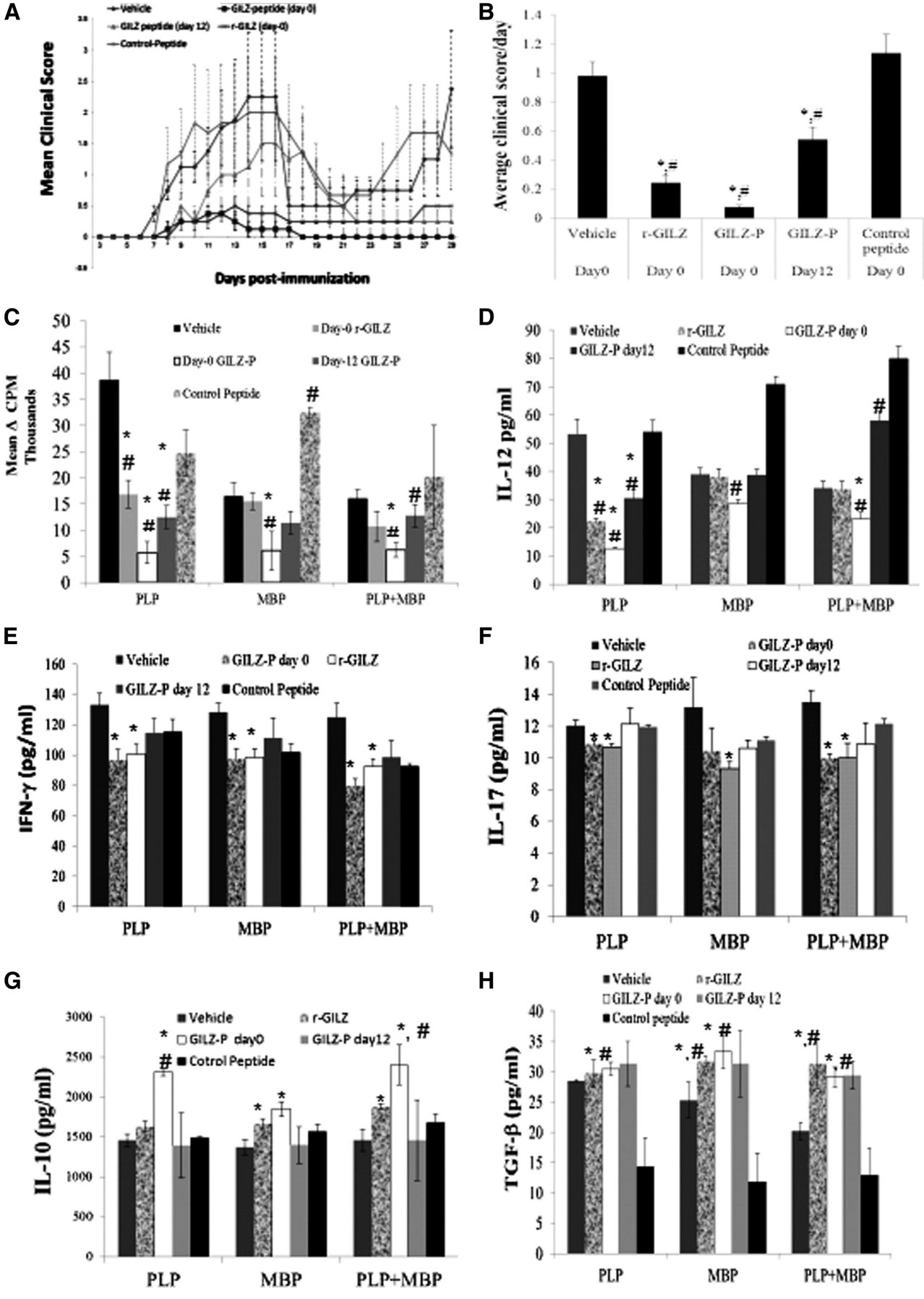
A
Vehicle
GILZ-peptide (day 0)
GILZ peptide (day 12)
r-GILZ (day 0)
Control-Peptide
Mean Clinical Score
Days post-immunization
B
Average clinical score/day
Vehicle
r-GILZ
GILZ-P
GILZ-P
Control peptide
Day0
Day 0
Day 0
Day12
Day 0
C
Mean Δ CPM Thousands
Vehicle
Day-0 r-GILZ
Day-0 GILZ-P
Day-12 GILZ-P
Control Peptide
PLP
MBP
PLP+MBP
D
IL-12 pg/ml
Vehicle
r-GILZ
GILZ-P day 0
GILZ-P day12
Control Peptide
PLP
MBP
PLP+MBP
E
IFN-γ (pg/ml)
Vehicle
GILZ-P day 0
r-GILZ
GILZ-P day 12
Control Peptide
PLP
MBP
PLP+MBP
F
IL-17 (pg/ml)
Vehicle
GILZ-P day0
r-GILZ
GILZ-P day12
Control Peptide
PLP
MBP
PLP+MBP
G
IL-10 (pg/ml)
Vehicle
r-GILZ
GILZ-P day0
GILZ-P day12
Cotrol Peptide
PLP
MBP
PLP+MBP
H
TGF-β (pg/ml)
Vehicle
r-GILZ
GILZ-P day 0
GILZ-P day 12
Control peptide
PLP
MBP
PLP+MBP

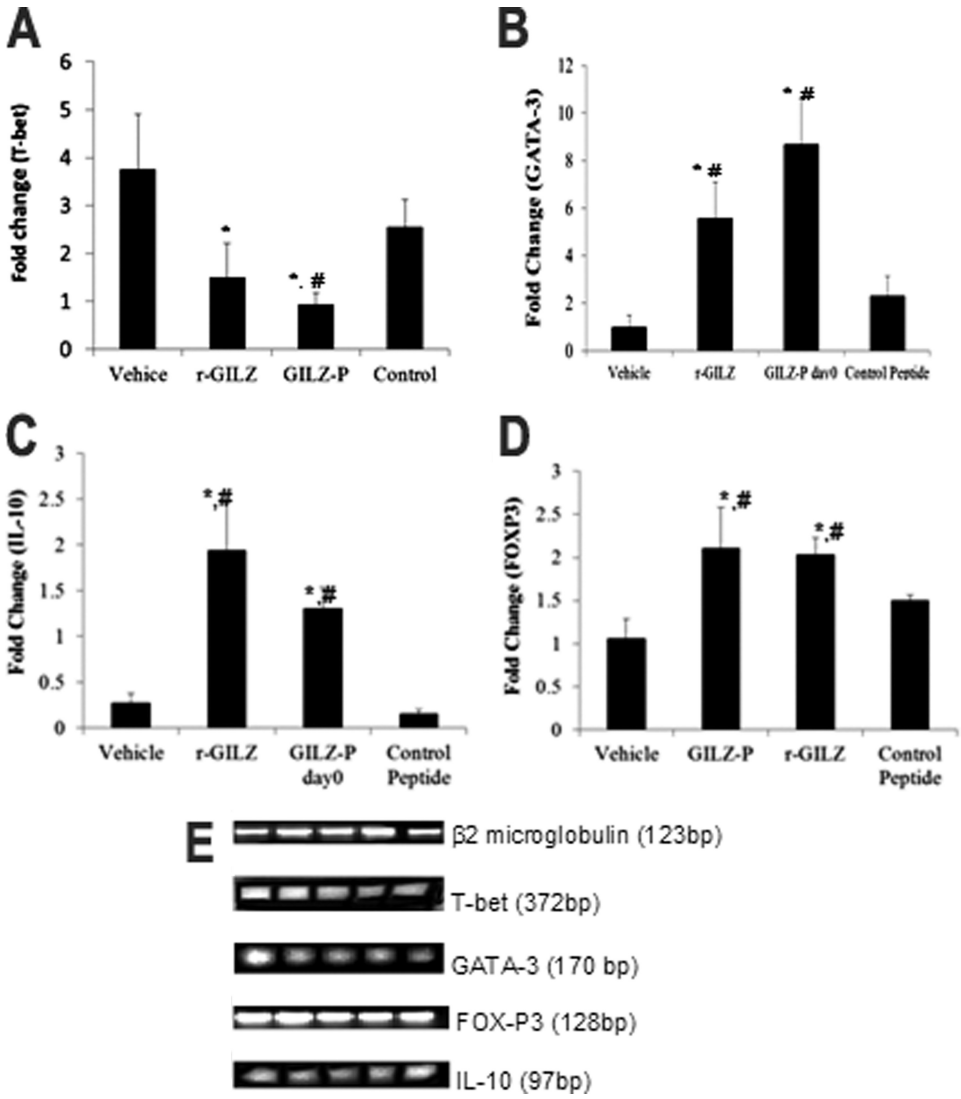

FIGURE 5. **GILZ-peptide treatment suppresses Th1 and enhances Th2 transcription factors in R-EAE.** CD4+ LNC isolated 45 days post-immunization from the draining lymph nodes of SJL/J mice induced with R-EAE and treated with GILZ-peptide (500 μg) either on day 0 with vehicle, r-GILZ, control-P, or vehicle (PBS) or on day 12 with GILZ-P ($n = 9$/group) were restimulated *in vitro* with $PLP_{139-151}$ (40 mg/ml) using syngenic irradiated splenocytes as APC in transwell systems. 50 ng of cDNA from CD4+ LNC were used for quantitative measurement of message for (*A*) T-bet, (*B*) GATA-3, (*C*) IL-10, and (*D*) FoxP3 by quantitative RT-PCR. *E*, gel electrophoresis of representative products. * and # represent $p < 0.05$ by analysis of variance as compared with vehicle or control peptide-treated group, respectively.

Targeted inhibition of the NF-κB complex is an actively investigated strategy to control inflammation (16). Previous approaches include interference with DNA binding by decoy nucleotides, blocking nuclear translocation by NF-κB dimers, inhibiting signaling kinases, and use of proteasome inhibitors (45). The NF-κB subunits also interact with multiple transcriptional regulators of cellular proliferation and apoptosis (45). The expanding network of NF-κB interactors has increased the potential for identifying newer targets for specific inhibition. In this study, we conceptually integrated the mechanism of action of glucocorticoids with the knowledge derived from the structural analysis of GILZ and its interaction with the p65 subunit of NF-κB in the design of GILZ-P, a bioactive synthetic peptide that exhibited therapeutic efficacy in a mouse model of human MS. The low molecular weight GILZ-P can provide promising leads for developing small molecule NF-κB inhibitors (4).

FIGURE 4. **GILZ-peptide treatment inhibits R-EAE.** SJL/J mice induced with R-EAE were administered intraperitoneally GILZ-peptide (500 μg) either on day 0 or 12 for r-GILZ (2 ng) and control peptide (500 μg) in complex with Pep-1 (0.3 μM) or Pep-1 alone, or vehicle (PBS) on the day of immunization. *A* shows the mean clinical score per day per group. *B*, the severity of EAE is depicted as the mean score per day, which is the cumulative score for each animal divided by the number of days that animal was observed. Data represent average ± S.D. from two experiments ($n = 9$/group). *C–H*, GILZ-peptide treatment suppresses Th1 cytokines in R-EAE. CD4+ splenocytes isolated 45 days post-immunization from the draining lymph nodes of SJL/J mice induced with R-EAE and treated with GILZ-peptide (500 μg) either on day 0 or 12 for r-GILZ, control peptide, or vehicle (PBS) were restimulated *in vitro* with $PLP_{139-151}$ (40 μg/ml), MBP_{87-99} (40 μg/ml), or both using syngenic irradiated splenocytes as APC for a total of 72 h (including an 18-h pulse with [^{3}H]thymidine). *C*, proliferative responses of CD4+ splenocytes are plotted as Δcpm ± S.E. #, $p < 0.05$ as compared with the responses of cells from vehicle-treated mice. Supernatant collected at 48 h from separate CD4+ splenocyte cultures were assessed for (*D*) IL-12, (*E*) IFN-γ, (*F*) IL-17, (*G*) IL-10, and (*H*) TGF-β by ELISA. * and # represent $p < 0.05$ as compared with vehicle or control peptide-treated groups, respectively.

REFERENCES

1. Martino, G. A., Furlan, R., and Poliani, P. L. (1999) in *Basic Immunology to Immune-mediated Demyelination* (Martino, G. A., Furlan, R., and Poliani, P. L., eds) Vol. 1, pp. 185–206, Springer, New York
2. van der Merwe, P. A., and Davis, S. J. (2003) *Annu. Rev. Immunol.* **21,** 659–684
3. Rath, A., Davidson, A. R., and Deber, C. M. (2005) *Biopolymers* **80,** 179–185
4. Sillerud, L. O., and Larson, R. S. (2005) *Curr. Protein Pept. Sci.* **6,** 151–169
5. Ravi Chandra, B., Gowthaman, R., Raj Akhouri, R., Gupta, D., and Sharma, A. (2004) *Protein Eng. Des. Sel.* **17,** 175–182
6. Bochicchio, B., and Tamburro, A. M. (2002) *Chirality* **14,** 782–792
7. Srinivasan, M., Lu, D., Eri, R., Brand, D. D., Haque, A., and Blum, J. S. (2005) *J. Biol. Chem.* **280,** 10149–10155
8. Srinivasan, M., Wardrop, R. M., Gienapp, I. E., Stuckman, S. S., Whitacre, C. C., and Kaumaya, P. T. (2001) *J. Immunol.* **167,** 578–585
9. Tanaka, K., Fujimoto, Y., Suzuki, M., Suzuki, Y., Ohtake, T., Saito, H., and Kohgo, Y. (2001) *Jpn. J. Cancer Res.* **92,** 959–967
10. Cannarile, L., Zollo, O., D'Adamio, F., Ayroldi, E., Marchetti, C., Tabilio, A., Bruscoli, S., and Riccardi, C. (2001) *Cell Death Differ.* **8,** 201–203
11. D'Adamio, F., Zollo, O., Moraca, R., Ayroldi, E., Bruscoli, S., Bartoli, A., Cannarile, L., Migliorati, G., and Riccardi, C. (1997) *Immunity* **7,** 803–812
12. Ayroldi, E., Migliorati, G., Bruscoli, S., Marchetti, C., Zollo, O., Cannarile, L., D'Adamio, F., and Riccardi, C. (2001) *Blood* **98,** 743–753
13. Cannarile, L., Fallarino, F., Agostini, M., Cuzzocrea, S., Mazzon, E., Vacca, C., Genovese, T., Migliorati, G., Ayroldi, E., and Riccardi, C. (2006) *Blood* **107,** 1039–1047
14. Ayroldi, E., and Riccardi, C. (2009) *FASEB J.* **23,** 3649–3658
15. Delfino, D. V., Agostini, M., Spinicelli, S., Vacca, C., and Riccardi, C. (2006) *Int. Immunopharmacol.* **6,** 1126–1134
16. Calzado, M. A., Bacher, S., and Schmitz, M. L. (2007) *Curr. Med. Chem.* **14,** 367–376
17. Di Marco, B., Massetti, M., Bruscoli, S., Macchiarulo, A., Di Virgilio, R., Velardi, E., Donato, V., Migliorati, G., and Riccardi, C. (2007) *Nucleic Acids Res.* **35,** 517–528
18. Schmitz, M. L., dos Santos Silva, M. A., Altmann, H., Czisch, M., Holak, T. A., and Baeuerle, P. A. (1994) *J. Biol. Chem.* **269,** 25613–25620
19. O'Shea, J. M., and Perkins, N. D. (2008) *Biochem. Soc. Trans.* **36,** 603–608
20. Gerritsen, M. E., Williams, A. J., Neish, A. S. Moore, S., Shi, Y., and Collins, T. (1997) *Proc. Natl. Acad. Sci. U.S.A.* **94,** 2927–2932
21. Lee, S. K., Kim, J. H., Lee, Y. C., Cheong, J., and Lee, J. W. (2000) *J. Biol. Chem.* **275,** 12470–12474
22. Asamitsu, K., Tetsuka, T., Kanazawa, S., and Okamoto, T. (2003) *J. Biol. Chem.* **278,** 26879–26887
23. Schmitz, M. L., Stelzer, G., Altmann, H., Meisterernst, M., and Baeuerle, P. A. (1995) *J. Biol. Chem.* **270,** 7219–7226
24. Dudhgaonkar, S. P., Janardhanam, S. B., Kodumudi, K. N., and Srinivasan, M. (2009) *J. Immunol.* **183,** 7505–7513
25. Nielsen, M., Lundegaard, C., Lund, O., and Petersen, T. N. (2010) *Nucleic Acids Res.* **38,** W576–581
26. Combet, C., Jambon, M., Deléage, G., and Geourjon, C. (2002) *Bioinformatics* **18,** 213–214
27. Kopp, J., and Schwede, T. (2004) *Nucleic Acids Res.* **32,** D230–234
28. Roy, A., Kucukural, A., and Zhang, Y. (2010) *Nat. Protoc.* **5,** 725–738
29. Seidel, G., Adermann, K., Schindler, T., Ejchart, A., Jaenicke, R., Forssmann, W. G., and Rösch, P. (1997) *J. Biol. Chem.* **272,** 30918–30927
30. Benkert, P., Tosatto, S. C., and Schomburg, D. (2008) *Proteins* **71,** 261–277
31. Srinivasan, R., and Rose, G. D. (1999) *Proc. Natl. Acad. Sci. U.S.A.* **96,** 14258–14263
32. Vanderlugt, C. L., Begolka, W. S., Neville, K. L., Katz-Levy, Y., Howard, L. M., Eagar, T. N., Bluestone, J. A., and Miller, S. D. (1998) *Immunol. Rev.* **164,** 63–72
33. Gros, E., Deshayes, S., Morris, M. C., Aldrian-Herrada, G., Depollier, J., Heitz, F., and Divita, G. (2006) *Biochim. Biophys. Acta* **1758,** 384–393
34. Morris, M. C., Depollier, J., Mery, J., Heitz, F., and Divita, G. (2001) *Nat. Biotechnol.* **19,** 1173–1176
35. Friguet, B., Chaffotte, A. F., Djavadi-Ohaniance, L., and Goldberg, M. E. (1985) *J. Immunol. Methods* **77,** 305–319
36. Heinrich, L., Tissot, N., Hartmann, D. J., and Cohen, R. (2010) *J. Immunol. Methods* **352,** 13–22
37. Dunker, A. K., Lawson, J. D., Brown, C. J., Williams, R. M., Romero, P., Oh, J. S., Oldfield, C. J., Campen, A. M., Ratliff, C. M., Hipps, K. W., Ausio, J., Nissen, M. S., Reeves, R., Kang, C., Kissinger, C. R., Bailey, R. W., Griswold, M. D., Chiu, W., Garner, E. C., and Obradovic, Z. (2001) *J. Mol. Graph. Model.* **19,** 26–59
38. Weber, M. S., Benkhoucha, M., Lehmann-Horn, K., Hertzenberg, D., Sellner, J., Santiago-Raber, M. L., Chofflon, M., Hemmer, B., Zamvil, S. S., and Lalive, P. H. (2010) *PLoS One* **5,** e16009
39. Saladin, P. M., Zhang, B. D., and Reichert, J. M. (2009) *IDrugs* **12,** 779–784
40. Zimecki, M. (2008) *Adv. Exp. Med. Biol.* **606,** 241–250
41. Bhattacharyya, R., and Chakrabarti, P. (2003) *J. Mol. Biol.* **331,** 925–940
42. Ayroldi, E., Zollo, O., Bastianelli, A., Marchetti, C., Agostini, M., Di Virgilio, R., and Riccardi, C. (2007) *J. Clin. Invest.* **117,** 1605–1615
43. Beaulieu, E., and Morand, E. F. (2011) *Nat. Rev. Rheumatol.* **7,** 340–348
44. Cannarile, L., Cuzzocrea, S., Santucci, L., Agostini, M., Mazzon, E., Esposito, E., Muià, C., Coppo, M., Di Paola, R., and Riccardi, C. (2009) *Gastroenterology* **136,** 530–541
45. Pande, V., and Ramos, M. J. (2005) *Curr. Med. Chem.* **12,** 357–374
46. Chenna, R., Sugawara, H., Koike, T., Lopez, R., Gibson, T. J., Higgins, D. G., and Thompson, J. D. (2003) *Nucleic Acids Res.* **31,** 3497–3500